Compatibilized iPP/aPS Blends: The Effect of the Viscosity Ratio of the Components on the Blends Morphology

Miroslav Slouf,[1] Gregor Radonjic,[2] Drahomira Hlavata,[1] Antonin Sikora[1]

[1]*Institute of Macromolecular Chemistry, Academy of Sciences of the Czech Republic, Prague, Czech Republic*
[2]*University of Maribor, FEB Maribor, Institute of Technology, Maribor, Slovenia*

Received 8 October 2004; accepted 26 August 2005
DOI 10.1002/app.23571
Published online in Wiley InterScience (www.interscience.wiley.com).

ABSTRACT: More than 25 PP/PS/SEP blends, where PP is isotactic polypropylene, PS is atactic polystyrene, and SEP is poly(styrene-*block*-ethylene-*co*-propylene), were prepared. The main objective of this study was to investigate the influence of PP/PS viscosity ratio, λ_{TM}, on the blends' morphology. It was shown that λ_{TM} strongly influenced not only the overall morphology of the blends, but also the morphology of SEP, which exhibited as many as five different types of structure when blended with PP and/or PS. SEP was found an efficient compatibilizer of PP/PS blends as it decreased the average particle size in all studied systems. An interesting "by-product" of this work was the discovery of a brand-new type of polymer morphology, which was called morel structure. The characteristic feature of the morel structure was PS matrix compartmentalized by SEP. © 2006 Wiley Periodicals, Inc. J Appl Polym Sci 101: 2236–2249, 2006

Key words: polymer blends; morphology; compatibilization; viscosity

INTRODUCTION

Polymer blending is a convenient route for the development of new polymer materials, which combine the properties of several single polymers. Since most blended polymers are immiscible, compatibilization is required to reduce coalescence, to lower interfacial tensions between components, and to improve the phase adhesion.

The shape, size, and spatial distribution of the phases in polymer blends result from a complex interplay between viscosity (and elasticity) of the blend components, their interfacial properties, blend composition, and processing conditions, as shown in a number of previous studies. It is generally agreed that among different factors, the viscosity ratio λ (i.e., the ratio between the viscosity of the dispersed polymer versus the viscosity of the matrix polymer) turned out to be one of the most critical variables in controlling the blend morphology.[1–14] A high viscosity ratio in many cases resulted in coarse morphology, while matching the viscosities ($\lambda \approx 1$) may result in much finer morphology,[1,6,7] although the general consideration of a minimum occurring when $\lambda \approx 1$ is not universally true. The diameter of dispersed particles in polycarbonate/polypropylene blends increased by a factor of 3–4 times, in the interval $\lambda = 4.5$–17.3.[9] Reduction in the size of the minor phase particles in same blends was achieved below $\lambda = 1$, with the minimum particle size occurring at $\lambda \approx 0.25$. Moreover, λ plays also a very important role in the process of the blend phase-inversion.[5,12,14]

Several theoretical and experimental studies have been performed to explain these processes, starting with the pioneering work of Taylor.[15,16] The dimensionless parameter, known as the capillary (or Weber) number ($Ca = R\eta_m\gamma/\sigma$, where R is characteristic size of the dispersed droplet, η_m the viscosity of the matrix, γ shear rate, and σ the interfacial tension), is often used for describing the size of the dispersed particles in polymer blends. Droplet breakup should occur at a critical Ca value (Ca_c). In the case of viscoelastic systems, Wu[7] has proposed an empirical relationship between Ca and λ as an adaptation of a more general equation, derived for the droplet size reduction in mixtures of Newtonian liquids, based on the studies on the droplet deformation and breakup for blends of polyamide and poly(ethylene terephthalate) with ethylene/propylene elastomers. Wu introduced the following equation, which relates interfacial tension σ and viscosity ratio λ:

$$\gamma d \eta_m / \sigma = 4\lambda^k \quad (1)$$

where d is the number–average diameter of dispersed particles. Parameter k is equal to $+0.84$ when $\lambda > 1$, and to -0.84 when $\lambda < 1$. From eq. (1), it is inferred

Correspondence to: M. Slouf (slouf@imc.cas.cz).
Contract grant sponsor: Grant Agency of the Czech Republic; contract grant numbers: 106/02/P029 and 106/02/1248.

that the reduction in particle size for the dispersed phase also results from a decrease in interfacial tension, which might be the result of interactions due to the localization of the compatibilizer in the interfacial regions.

It is known that the shear and temperature fields (which influence the viscosities) are not the same in internal mixers and capillary rheometers. Therefore, different authors who prepared their samples with internal mixers rather used the concept of torque ratio than the viscosity ratio. Since there is a correlation between torque and viscosity, such concept is admissible.[8,9,17–19]

An effective compatibilizer affects deformation and breakup of dispersed particles by reducing the interfacial tension, and thereby lowers the hydrodynamic stress at which drops of certain size break.[3,7,19–21] The compatibilizer activity of block copolymers may be influenced by the viscosity ratio of the blend components as reported in various studies. Taha and Frerejean[22] observed that compatibilization effectiveness of styrene–rubber block copolymers was higher in low-density polyethylene/polystyrene 75/25 blend when $\lambda \approx 1$ compared to that of the same blend with $\lambda > 1$. Willis et al.[10] showed that the interfacial modification in polypropylene/polyamide and polyethylene/polyamide blends caused by the addition of an ionomeric compatibilizer diminished the dependence of the dispersed phase particle size on the viscosity ratio of the blend.

Immiscible isotactic polypropylene (iPP)/atactic polystyrene (aPS) blends can exhibit a variety of different phase morphologies depending on the weight ratio of iPP and aPS, rheological properties, and processing conditions. Han et al.[23] found that even moderately different modes of dispersion and particle size can give rise to pronounced differences in the apparent rheological properties in the molten state of the binary iPP/aPS blends. Miroshnikov and Williams[24] reported on wide diversity of phase structures in iPP/aPS extrudates with aPS matrix in the viscosity ratio interval $0.09 < \lambda < 5.5$. Their work also supported the fact that processing conditions, elasticity effects, and interfacial tension have to be considered in explaining final phase morphologies. Fortelný et al.[25] and Navrátilová and Fortelný[26]; showed that the average aPS particle sizes in binary iPP/aPS blends decrease with increasing viscosity of the iPP matrix. Dispersed particles became more elongated in the case of $\lambda < 1$. This is in accordance with some proposed morphological models.[6] Coalescence was found to be the faster when the viscosity of the dispersed phase or the matrix was lower. Fujiyama observed that the viscosity ratio also influenced the final morphology of binary iPP/aPS blends prepared by injection molding.[27] He reported that PS particles were large when λ was higher or lower than 1 and were smallest when λ was slightly lower than 1. In recent years, studies, both theoretical and experimental,[25,26,28–34] of the compatibilization aspects in blends of aPS and iPP have been the center of interest. A series of block copolymers (BC) with polystyrene blocks and with rubber blocks of aliphatic hydrocarbons were used in these studies. Different factors and aspects that seemed to be influential regarding the morphology development and final properties were systematically studied, like weight ratio of the basic components, type and content of the styrene block copolymers, the number of blocks in the block copolymers, the length of the blocks in block copolymers, and the time and the rate of blending. These studies confirmed that a compatibilization process in iPP/aPS blends is very complex with many influential factors determining the final properties. It was also been shown that among styrenic-rubber block copolymers (SRBC), diblock copolymer poly(styrene-*block*-ethylene-*co*-propylene) (SEP) was an efficient compatibilizer for immiscible iPP/aPS blends, especially when iPP was a matrix phase.[35,36] Moreover, phase morphology showed some interesting features, such as the bimodality of the dispersed particles even when SEP completely enveloped dispersed aPS particles as well as the tendency of clustering of the dispersed particles when the content of SEP was increased up to 10 wt %.

Since the majority of the reported studies relatively well describe the influence of the viscosity ratio on the phase morphology of iPP/aPS and other binary blends, the emphasis in this paper is given to the effect of how the viscosity ratio influences interfacial activity of SEP block copolymer and final morphology of the compatibilized iPP/aPS blend, which was not widely studied yet.

EXPERIMENTAL

Materials and blend preparation

Two different grades of iPP and two of aPS were used in this study. The polypropylenes were Daplen BM 55 (PP-2 in the following text), and noncommercial low-viscous iPP (PP-3), both produced by ÖMV-PCD Polymere (Austria). The polystyrenes were GP 678E (PS-1; DOKI, Croatia) and 168N (PS-2; BASF, Germany). Linear diblock copolymer SEP, produced by Shell Chem Co. under the commercial name Kraton G-1701, was used as a compatibilizer. The polymer characteristics are summarized in Table I.

PS pellets were dried overnight at 70°C before use and premixed with iPP and SEP pellets before being fed into the kneading chamber. Blends of different compositions were prepared by melt blending in an oil-heated Brabender kneading chamber at 200°C for 6 min, with a rotor speed of 50 rpm. After finishing the blending process, they were transferred rapidly between two aluminum sheets placed in a hydraulic

TABLE I
Characteristics of Used Polymers

Polymer	M_n[a] (g/mol)	M_w/M_n[a]	MFI (g/10 min)	Torque[d] (N m)	φ (PS) (wt %)
PP-2	113,450	3.2	0.7[b]	25	—
PP-3	58,905	2.0	61.3[b]	5	—
PS-1	96,000	2.4	12.5[c]	11	—
PS-2	175,000	2.1	1.7[c]	20	—
SEP	89,500	1.5	0.6[c]	—	37.0[e]

[a] Measured by size exclusion chromatography.
[b] ASTM D 1238 (230°C/2.16 kg).
[c] ASTM D 1238 (200°C/5 kg).
[d] After 6 min in Brabender kneading chamber at 200°C with rotor speed 50 rpm.
[e] Manufacturer's data.

press preheated to 220°C. Samples of blends used for morphological investigations were prepared by compression molding. A load of 100 bar was used, and after 10 min 1-mm-thick plates were removed and cooled to room temperature in air. Both noncompatibilized and compatibilized PP/PS blends with weight ratios 80/20 and 20/80 were examined; amount of SEP in compatibilized blends varied from 2.5 to 10 wt %. Additionally, pure SEP, binary blends PP/SEP and PS/SEP, and a few PP/PS/SEP blends with other weight ratios of the components were prepared using the same procedure.

Rheological measurements

The viscosity values of neat polymers were obtained with a capillary extrusion rheometer Göttfert Rheograph at 200°C. The rheometer had an L/D ratio of 20/1 (Table I). The plots of the shear viscosity (η) versus shear rate (γ) of neat components have already been published.[37]

Since the complex geometry of the Brabender kneading chamber and different shear stress as well as temperature gradients inside the chamber make direct conversion of capillary rheometer tests inaccurate, we believe it is more convenient to use the values of torques as a rheological parameter in this study. By using the torque ratio as the viscoelastic characteristic of the materials, shearing and elongational forces that act on the polymers during blending in an internal mixer are included.

The torque values reported in the text were measured in a Brabender kneading chamber at 200°C with a rotor speed of 50 rpm; constant values were reached after 6 min of mixing. Torque values for the pure materials are given in Table I. Torque ratio was calculated using the torque values for pure components from the following equation:

$$\lambda_{TM} = \left.\frac{M_d}{M_m}\right|_{n,T,t} \quad (2)$$

where λ_{TM} is the torque ratio, M_d is the torque value of the polymer which constitutes a dispersed phase, M_m is the torque value of the polymer which constitutes a matrix phase, n is the rotor speed, T is the temperature, and t is the time of mixing. On the basis of the torque values of the neat polymers, we determined the torque ratios for the various PP/PS blends as follows: λ_{TM} = PS-1/PP-2 = 0.4, λ_{TM} = PS-2/PP-3 = 4.0, λ_{TM} = PP-2/PS-1 = 2.5, and λ_{TM} = PP-3/PS-2 = 0.25.

Electron microscopy

Scanning electron microscopy (SEM) was performed with JSM 6400 microscope (Jeol, Japan). Samples were immerged in liquid nitrogen, left to equilibrate 5 min, fractured, sputtered with platinum, and observed in the microscope at 25 kV, using secondary electron detector.

Scanning transmission electron microscopy (STEM) was carried out with Vega TS 5130 microscope (Tescan, Czech Republic), equipped with a transmission adapter. Ultrathin sections of the samples were cut with ultramicrotome Ultracut UCT (Leica, Austria) at −140°C, stained with RuO_4 vapors for ~20 min, and observed in the microscope at 30 kV, using transmission detector.

Transmission electron microscopy (TEM) was performed with JEM 200CX microscope (Jeol, Japan). Samples for TEM were prepared in the same way as the samples for STEM. TEM micrographs were exposed at 100 kV. In both STEM and TEM micrographs of RuO_4-stained ultrathin sections PP appeared white, PS appeared gray, and SEP appeared black. On a few micrographs it was observed that PS was darker than SEP; this occurred if longer staining times were used and so it might have been caused because SEP was stained less intensively but faster, whereas PS was stained more intensively but more slowly.

Small-angle X-ray scattering

Small-angle X-ray scattering (SAXS) measurements were performed using an upgraded Kratky camera, with a 60-μm entrance slit and 42-cm flight path. Ni-filtered CuKα radiation (wavelength λ = 1.54 Å) was used and registered with a position-sensitive detector[38] (Joint Institute for Nuclear Research, Dubna, Russia), for which the spatial resolution is ~0.15 mm. The intensities were taken in the range of the scattering vector $q = (4/\pi) \sin \theta/\lambda$ from 0.006 to 0.2 Å^{-1} (where 2θ is the scattering angle). The measured intensities were corrected for sample thickness and transmission, primary beam flux, and sample-detector distance, but not for slit collimation effects.

RESULTS

This work deals with PP/PS blends compatibilized with SEP. Some of the studied blends contained such

TABLE II
Summary of Key Studied Blends and Their Morphology

PP/PS/SEP blends		Particle size	Morphology of compatibilized blend
$\lambda_{TM} = 4$	PP/PS (80/20)	5–20 μm	PP matrix with PS particles connected by SEP
	+10% of SEP	0.5–4 μm	having ordered supramolecular structure.
$\lambda_{TM} = 0.4$	PP/PS (80/20)	1–6 μm	PP matrix with PS particles connected by
	+10% of SEP	0.1–1 μm	swollen SEP having ordered supramolecular structure.
$\lambda_{TM} = 2.5$	PP/PS (20/80)	1–20 μm	PS matrix with PP particles enveloped by
	+10% of SEP	0.1–1 μm	SEP; a part of SEP dispersed in PS matrix.
$\lambda_{TM} = 0.25$	PP/PS (20/80)	1–50 μm	PS matrix compartmentalized by SEP into
	+10% of SEP	0.5–10 μm	cells; some cells filled with PP. Morel structure.

a high amount of the compatibilizer that they could be regarded as ternary systems PP/PS/SEP. More than 25 different PP/PS/SEP blends with compositions $X/Y/Z$ and viscosity ratios λ_{TM} were examined. X/Y is weight percent of PP/PS, Z is weight percent of SEP, and λ_{TM} is viscosity ratio of PP/PS defined in experimental section. The polymers used for blend preparation are characterized in Table I and the most important of the prepared blends are summarized in Table II.

The morphology of the blends was investigated by EM and SAXS techniques. The combination of the two techniques proved to be very useful both in this work and some previous studies.[28–34] EM yields direct and detailed insight into blend morphology. SAXS experiments are usually much faster than EM experiments, but the information we get is indirect and should be confronted with other results. In this work, SAXS curves were interpreted by means of EM micrographs and a very good agreement was found. As soon as the features of SAXS curves were known, it was possible to study analogous systems only by means of routine SAXS experiments. Another advantage of SAXS is that the signal is collected from a larger region than in EM. Therefore the structure, which SAXS yields information about, is more averaged and the influence of exceptions on the SAXS signal is limited.

In the course of the work, some morphologies of PP/PS/SEP blends were found quite complicated. To understand factors influencing localization and structure of the compatibilizer in ternary blends, morphology of neat SEP and simpler binary blends were investigated as well. At certain concentrations and viscosity ratios of the PP/PS/SEP blend components, unusual *morel morphology* was observed. As we believed this morphology had not been observed yet, we prepared and investigated more blends to describe conditions under which the morel morphology is formed.

Neat SEP

Neat SEP has a lamellar structure as documented in Figure 1(a). SAXS curve of neat SEP (Fig. 2, dot line) shows strong maximum at the value of diffraction vector $q \approx 0.01$ Å^{-1}, very weak maximum at $q \approx 0.02$ Å^{-1}, and weak maximum at $q \approx 0.03^{-1}$Å. These maxima correspond to the ordered lamellar structure of separated polystyrene and poly(ethylene-*co*-propylene) blocks of SEP. SAXS interference distance calculated from Bragg Law ($2\pi/q = 540$ Å) agreed very well with the distance measured from STEM microphotographs (~530 Å). The following detail might be worth noting: when an measuring interference dis-

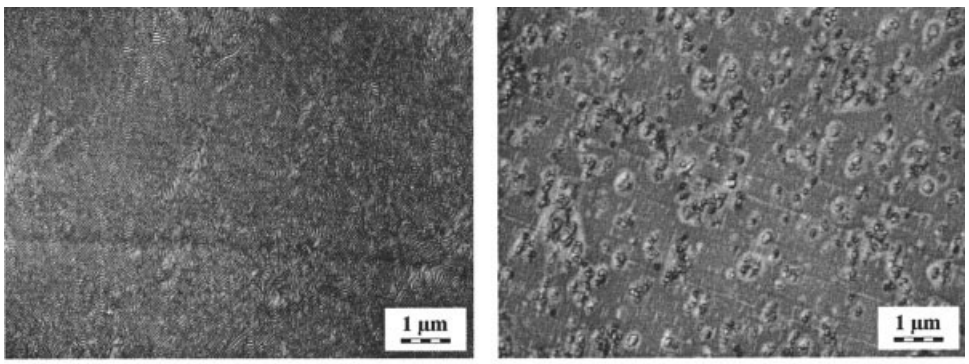

Figure 1 STEM micrographs of RuO_4-stained ultrathin sections of (a) neat SEP and (b) PP/SEP 90/10 blend.

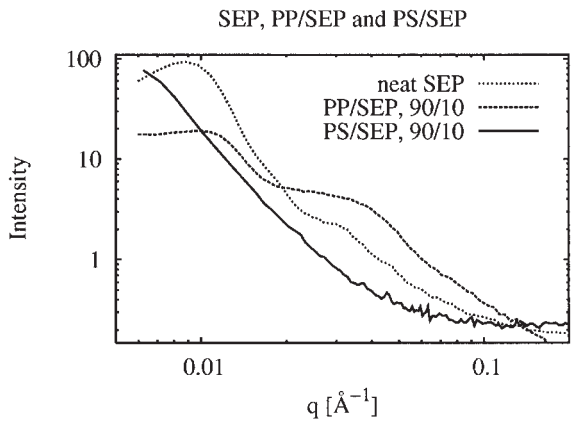

Figure 2 SAXS curves of neat SEP, PP/SEP, and PS/SEP blends.

tance from STEM microphotographs, we should consider the finite thickness of ultrathin sections and a possible tilt of SEP layers (characterized by tilt angle θ); if the layers were not perpendicular to ultrathin section normal, the measured interference distance would be $1/\cos(\theta)$ times higher than the actual interference distance. That is why it is necessary to find in the STEM micrograph a region with minimal distance between the layers and measure the interference distance in this region supposing that it holds $\theta = 0$ there.

Binary blends PP/SEP, PS/SEP, and PP/PS

The PP/SEP blends were studied by Radonjic and Smit[39] using microscopic techniques and in this work using SAXS. Light microscopy microphotographs showed PP matrix with SEP particles in all studied blends. TEM microphotographs of RuO_4-stained ultrathin sections suggested that SEP phase is formed by adjacent micelles with PS core and EP shell. Both core and shell dimensions were very close to the thickness of the layers of the lamellar structure of neat SEP. As the SEP micelles were adjacent to each other, SEP maintained its periodic microstructure in PP/SEP blends, although the SEP structure changed from lamellar to micellar. This was confirmed by SAXS experiments, performed in this study (Fig. 2), in which strong maximum at $q \approx 0.01$ Å^{-1} was observed for both neat SEP and all PP/SEP blends. The second maximum on SAXS curves of PP/SEP at $q \approx 0.04$ Å^{-1} corresponds to the long period of semicrystalline polymer iPP.

The PS/SEP blends morphology was different from that of PP/SEP blends as documented in Figure 1(b). The PS/SEP blends contained separated SEP micelles with the core–shell structure in PS matrix. With increasing concentration of SEP, the micelles tended to agglomerate. However, the agglomerates of SEP micelles were so small that no peak corresponding to internal structure of SEP was observed on SAXS curve (Fig. 2). The periodicity in SEP was completely lost. As the polymer aPS is amorphous, the SAXS curves of PS/SEP blends are monotonous, without any peaks.

All PP/PS blends (Fig. 3) show two-phase morphology with weak interfacial adhesion between particles of the minority component and matrix of the majority component. Their SAXS curves (Fig. 4) exhibit no special features. The peak at $q \approx 0.04$ Å^{-1} corresponds to long period of semicrystalline polymer iPP. The peak grows with increasing content of PP in the blend.

PP/PS blends with PP matrix ($X/Y = 80/20$, $\lambda_{TM} = 4$ and 0.4, Figs. 3(a) and 3(b)) contain PS particles with broad size distribution. In the blends with $\lambda_{TM} = 4$, many dispersed PS particles have diameters up to 50 μm, while in the $\lambda_{TM} = 0.4$ blends, much finer dispersion is obtained. It is interesting that in the case of $\lambda_{TM} = 0.4$ just a few rod-like dispersed particles were observed as opposed to other experimental studies of iPP/aPS blends.[26] However, if the content of PS is increased from 20 to 30 wt %, rod-like particles starts to appear, as proved by Radonjič.[40] It is worth mentioning that in the binary iPP/aPS blends with $\lambda \approx 1$, the average diameter of the dispersed aPS particles increased from 1.2 (in iPP/aPS 90/10 blend) to 6.9 μm (in iPP/aPS blend 70/30), confirming the importance of the weight ratio of the dispersed aPS phase on the morphology coarseness.

PP/PS blends with PS matrix ($X/Y = 20/80$, $\lambda_{TM} = 2.5$ and 0.25) contain only spherical or slightly ellipsoidal PP particles. Surprisingly enough, the size of the particles increases with increasing viscosity of the matrix (cf. Figs. 3(c) and 3(d)). This disagrees with both theoretical predictions and some experiments as summarized in the Introduction. On the one hand, it should be noted that the particle size distribution in PS–matrix blends is rather broad, with particle sizes slightly differing from place to place, which prevents precise particle size analysis. On the other hand, the same trend, i.e., larger particles in the blend with higher-viscosity matrix, was observed in compatibilized PP/PS/SEP blends (cf. Figs. 3(a) and 3(b) with 5(a) and 5(b)).

Compatibilized blends PP/PS/SEP

All PP/PS/SEP blends ($X/Y = 80/20$ and $20/80$, $Z = 10$) are shown in Figure 5. In all compatibilized blends, SEP reduced the average particle size in comparison with noncompatibilized systems, acting as a compatibilizing agent (Table II). The viscosity ratios, λ_{TM}, significantly influenced the blend morphology as confirmed by the confrontation of blends differing in this parameter only (cf. Figs. 5(a) and 5(c) with 5(b) and 5(d)).

The PP/PS/SEP blends with PP matrix contain dispersed PS particles enveloped and connected together with SEP. In the blends with $\lambda_{TM} = 4$, the dispersed

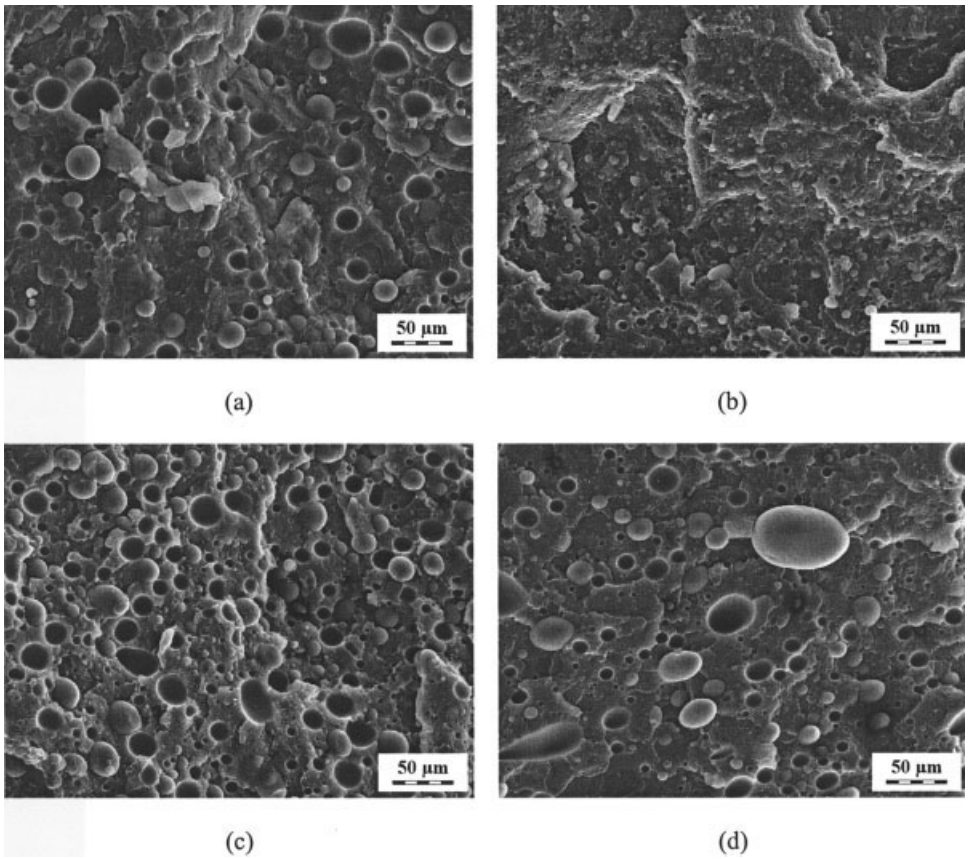

Figure 3 SEM micrographs of fracture surfaces of PP/PS binary blends: (a) PP/PS volume ratio 80/20, $\lambda_{TM} = 4$; (b) 80/20, $\lambda_{TM} = 0.4$; (c) 20/80, $\lambda_{TM} = 2.5$; and (d) 20/80, $\lambda_{TM} = 0.25$.

particles are clearly larger than for the $\lambda_{TM} = 0.4$. The PS particles tend to form aggregates in both blends with $\lambda_{TM} = 4$ and $\lambda_{TM} = 0.4$, which was observed in PP/PS/SEP blends with $\lambda \approx 1$ as well.[36] The SEP compatibilizer, enveloping and connecting PS particles, maintained its periodic microstructure to some extent. This was confirmed by TEM micrographs (Fig. 6) and SAXS measurements (Figs. 4(a) and 4(b)). In the PP/PS/SEP blend with $\lambda_{TM} = 4$, adjacent micelles of SEP, very similar to those observed and described in the binary PP/SEP blends,[39] are located between dispersed PS particles (Fig. 6(a)). SAXS curves (Fig. 4(a)) exhibit the maximum at $q \approx 0.01$ Å^{-1}, exactly as in the case of PP/SEP blends. In PP/PS/SEP blends with $\lambda_{TM} = 0.4$, the adjacent micelles of SEP are nonuniform and bigger than in the previous case (Fig. 6(b)) and, as a result, the maximum on the SAXS curves (Fig. 4(b)) broadens and shifts towards lower q. In fact, the average micelle size is so big that we could observe the maximum only partially in the form of decreasing curve slope in the region of lowest q values.

The PP/PS/SEP blends with PS matrix exhibited even deeper changes of their morphology with changing viscosities of the components. The blends with $\lambda_{TM} = 2.5$ showed standard morphology with PS matrix containing PP particles enveloped with SEP (Fig. 5(c)). Higher-magnification micrographs reveal that a small amount of SEP is probably dispersed in the PS matrix in the form of separated micelles, which were observed in PS/SEP blends (Fig. 1(b)). In any case, SEP lost its periodic microstructure completely, and consequently, the SAXS curves (Fig. 4(c)) showed no maxima corresponding to SEP internal structure. The only maximum on SAXS curves, observed at $q \approx 0.04$ Å^{-1}, is associated with the long period of PP. The blends with $\lambda_{TM} = 0.25$ exhibited quite a different morphology, which was called "morel structure" according to the texture observed on STEM micrographs of RuO_4-stained ultra-thin sections (Fig. 5(d)). The morel structure is characterized by thin sheets of SEP compatibilizer that form three-dimensional network penetrating through the PS matrix, compartmentalizing the matrix and wrapping the PP particles. According to the available literature, this unusual type of polymer morphology has not been described yet. The SAXS curve of morel structure (Fig. 7) contains maximum at $q \approx 0.04$ Å^{-1}, corresponding to the long period of PP, and exhibits decreasing slope in the region with $q < 0.01$ Å^{-1}, which is connected with scattering on SEP layers as discussed in the next section. The decrease in slope at $q < 0.01$ Å^{-1} seems to result from very broad and

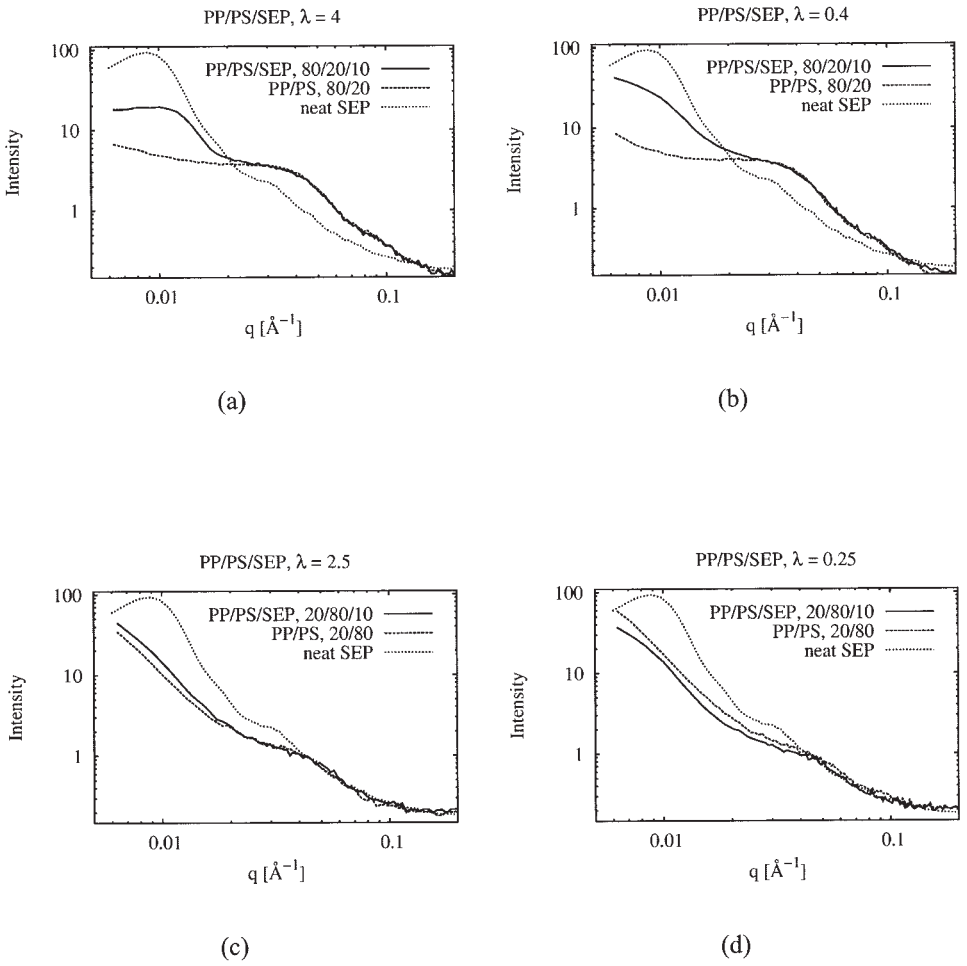

Figure 4 SAXS curves of PP/PS/SEP blends with different viscosity ratios: (a) $\lambda_{TM} = 4$, (b) $\lambda_{TM} = 0.4$, (c) $\lambda_{TM} = 2.5$ and (d) $\lambda_{TM} = 0.25$. The SAXS curve of neat SEP is given in each figure for comparison.

very low peak around $q \approx 0.008$ Å^{-1}; as this is not completely clear, the more general term *decreasing slope* is used in the following text.

Morel structure

To our knowledge, the morel structure is quite a novel type of polymer blend morphology. Its main feature is the *compartmentalized matrix*, which forms the characteristic morel texture on STEM micrographs (Figs. 5(d), 8(b)–(d), 9(b)). However, it should be noted that several blends with *compartmentalized particles* have been described. The well-known structure of HIPS (high-impact polystyrene) contains compartmentalized polybutadiene particles with morel-like structure[41] in PS matrix. Also in PP/PS/SBS blends[42] with PP matrix, PS particles compartmentalized by SBS (poly(styrene-*block*-butadiene-*block*-styrene) were observed.

Nevertheless, the compartmentalized matrix in PP/PS/SEP blends seems to be unique. That is why we tried to describe the conditions, under which it is formed, in more detail. The results of the microscopic analysis (Figs. 5, 8, and 9) prove that morel structure was not formed by coincidence; on the contrary, it develops at precisely defined conditions.

The first question concerning the morel structure is associated with the influence of the viscosity ratio on the morphology. This problem has already been discussed in the previous section. In any case, it should be reemphasized here that the morel structure was observed just at viscosity ratio $\lambda_{TM} = 0.25$ (Fig. 5(d)). The blend with the same composition, differing just in $\lambda_{TM} = 2.5$, exhibited completely different morphology (Fig. 5(c)).

The second question is, at which concentration of SEP the morel structure appears. To investigate this, a series of PP/PS/SEP blends with composition 20/80/Z, where Z stands for increasing concentration of SEP in wt %, were prepared. STEM micrographs prove that at $Z = 5$ wt % the SEP compatibilizer is localized mostly at PP/PS interface and partially in PS matrix (Fig. 8(a)), at $Z = 6.5$ wt % the morel structure starts to grow (Fig. 8(b)), at $Z = 8.5$ wt % it has already

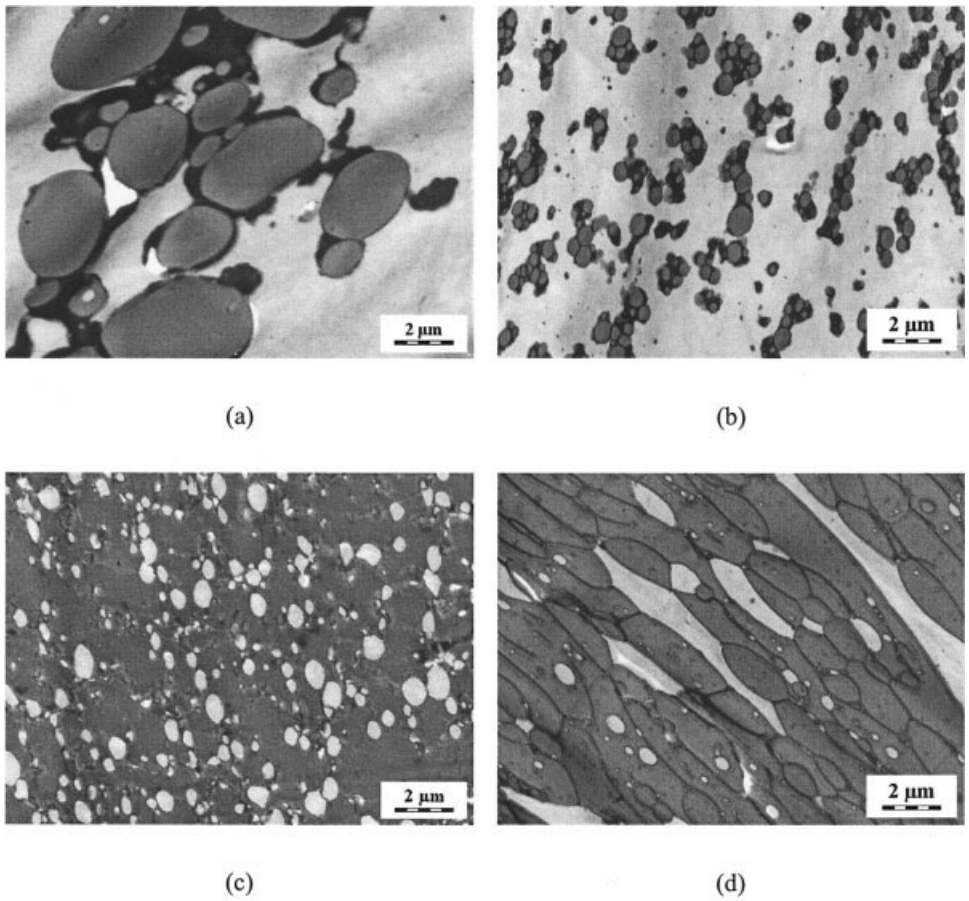

Figure 5 STEM micrographs of RuO_4-stained ultrathin sections of PP/PS/SEP blends: (a) 80/20/10, $\lambda_{TM} = 4$; (b) 80/20/10, $\lambda_{TM} = 0.4$; (c) 20/80/10, $\lambda_{TM} = 2.5$; and (d) 20/80/10, $\lambda_{TM} = 0.25$.

been developed (Fig. 8(c)), and at $Z = 10$ wt % (Fig. 5(d)) and $Z = 12.5$ wt % (Fig. 8(d)) it matures with increasing concentration of SEP. The morel structure impacts on the shape of SAXS curves (Fig. 7(a)): at $q < 0.01$ the slope of the curve decreases if the morel structure occurs. That is why the development of the morel structure can be observed also by SAXS, because the decrease in slope grows as the morel structure develops. At $Z = 5$ and 6.5 wt % the slope is more-or-less unchanged, at $Z = 8.5$ wt % the change in slope starts to be visible and this effect further amplifies with increasing Z. There are at least three possible explanations of this behavior: (i) the changed slope is caused by the scattering on SEP sheets and we observe

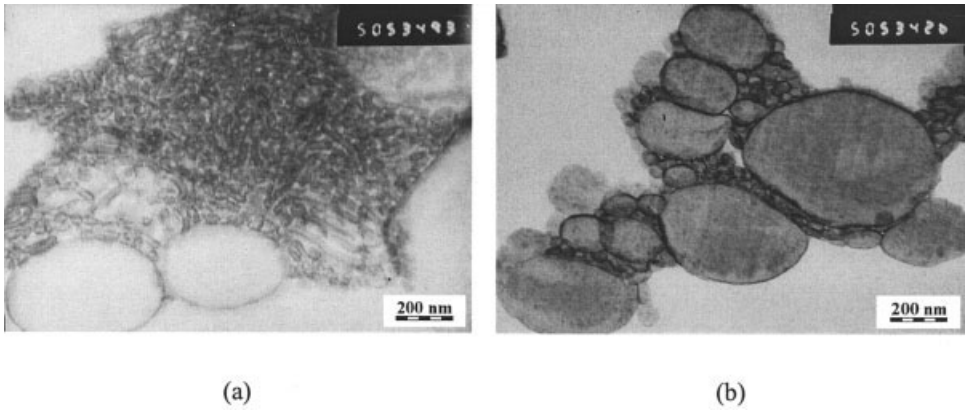

Figure 6 TEM micrographs of RuO_4-stained ultrathin sections of PP/PS/SEP (80/20/10) blends: (a) $\lambda_{TM} = 4$ and (b) $\lambda_{TM} = 0.4$.

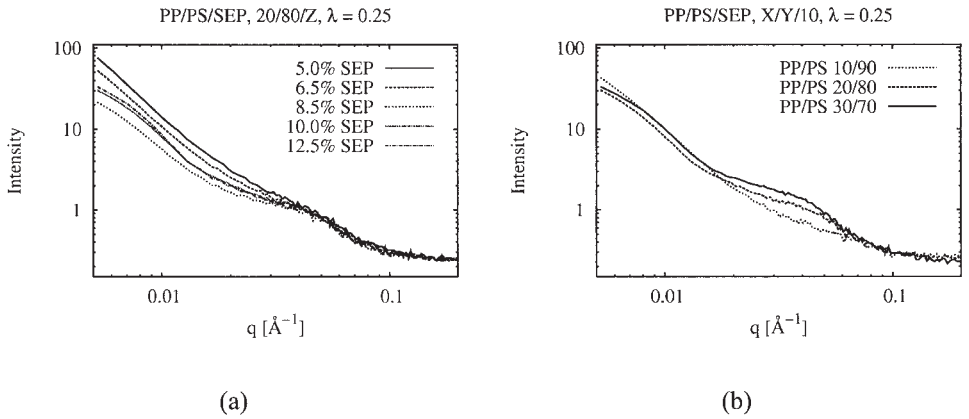

Figure 7 SAXS curves of PP/PS/SEP blends with $\lambda_{TM} = 0.25$, showing development of morel morphology: (a) influence of increasing SEP content and (b) influence of increasing PP/PS ratio.

second or higher maximum corresponding to scattering on finite thin sheets, (ii) the changed slope is connected with the scattering of cross sections of SEP sheets, and (iii) the effect was caused by the scattering on SEP sheets because scattering of a thin sheet exhibits lower slopes than corresponding scattering of spherical objects. Explanation (iii) looks wrong because the decrease in slope seems to be a broad and low peak. Explanation (ii) seems to be wrong as the peak does not shift with decreasing average distance among the cross sections, which lowers with Z. Therefore the explanation (i) might the correct one. Some

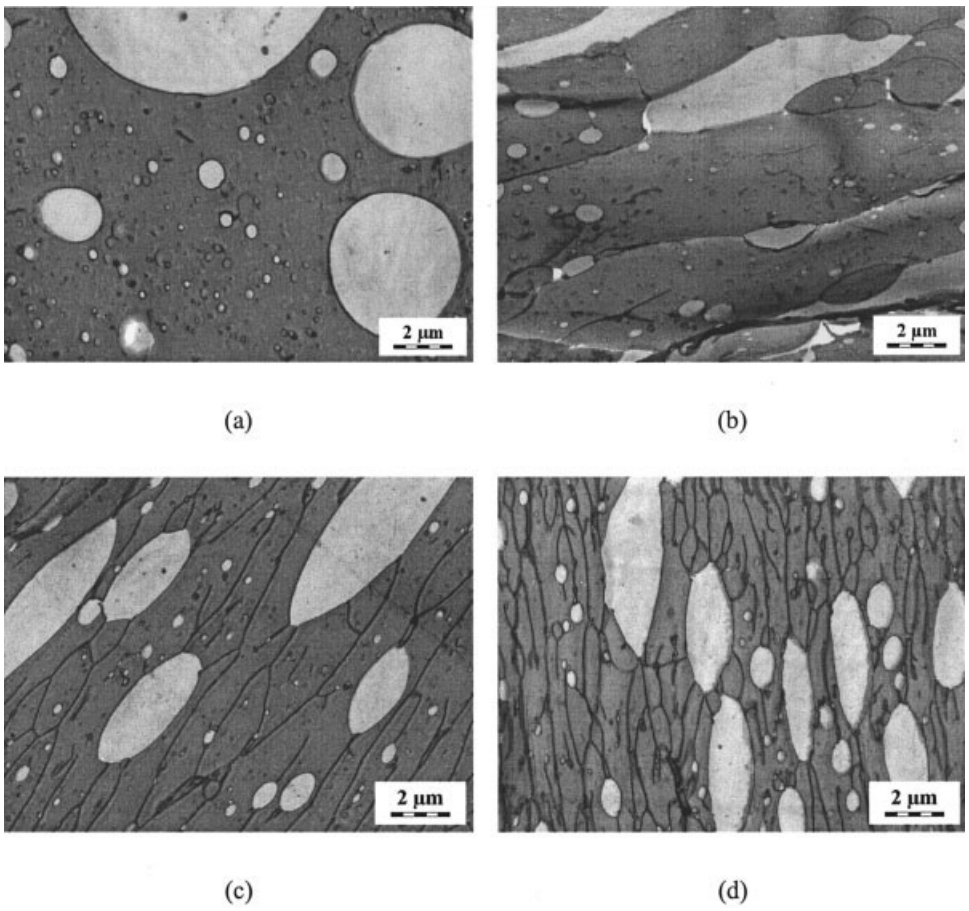

Figure 8 STEM micrographs of RuO_4-stained ultrathin sections of PP/PS/SEP (20/80/Z) blends, with $\lambda_{TM} = 0.25$ and Z equal to (a) 5 wt %, (b) 6.5 wt %, (c) 8.5 wt %, and (d) 12.5 wt %. Morel structure pronounces with increasing Z (see also Fig. 5(d)).

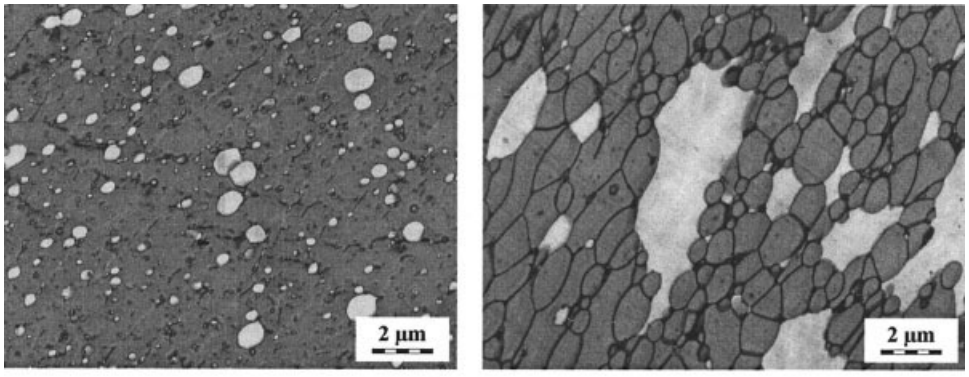

Figure 9 STEM micrographs of RuO_4-stained ultrathin sections of PP/PS/SEP ($X/Y/10$) blends, with $\lambda_{TM} = 0.25$ and X/Y equal to (a) 10/90 and (b) 30/70. Morel structure pronounces with increasing X/Y (see also Fig. 5(d)).

theoretical modeling or neutron scattering experiments with deuterated SEP could clarify this problem. Nevertheless, the basic fact that the change in slope at lowest q concerns the morel structure is evident.

The third question is, at which PP/PS weight ratios the morel structure starts to grow. In other words, will the morel structure arise also in binary PP/SEP blend or will it appear only in PP/PS/SEP blends containing certain amount of PP? The answer is shown in Figures 5(d) and 9, illustrating the development of morel structure in the blends PP/PS/SEP with composition $X/Y/10$, where X/Y stands for the increasing PP/PS weight ratio. At $X/Y = 10/90$ (Fig. 9(a)), the morel structure is not observed. PS matrix contains two kinds of particles: larger spherical PP particles enveloped with SEP and smaller irregular particles of neat SEP. At $X/Y = 20/80$ (Fig. 5(d)) the morel structure is formed and at $X/Y = 30/70$ (Fig. 9(b)) it is even amplified. The development of the morel structure can again be observed on SAXS curves indirectly, in the form of decreasing slope at the lowest q, as discussed in the previous paragraph. The SAXS curves of the PP/PS/SEP $X/Y/10$ blends (Fig. 7(b)) exhibit two features: (a) the slope decrease at the lowest q amplifies with increasing X/Y, which corresponds to more and more matured morel structure and (b) the peak at $q \approx 0.04$ Å^{-1}, associated with the long period of PP, grows with increasing X/Y as the amount of PP in the blend rises.

Several additional features, concerning morel structure, are worth noting: (a) Certain bimodality of the dispersed PP particles can be observed. Except for larger PP particles, there are a lot of small PP particles inside morel-like PS/SEP matrix. (b) The larger PP particles are rather elongated and the elongation seems to increase with growing morel structure. (c) SEP acts as a compatibilizing agent also in all blends exhibiting the bizarre morel structure because the average particle size definitely decreases in comparison with noncompatibilized blend (cf. Figs. 3(d) and 5(d)). (d) In agreement with theoretical assumptions, the average size of PP particles slightly decreases with SEP concentration and considerably increases with PP concentration as documented in Figures 5(d), 8, and 9.

Other studied blends

To understand and verify the results, several more PP/PS/SEP blends were studied using EM and SAXS. Some of the results were not shown in the previous sections to keep this paper brief and clear. These results are just listed here.

The PS/SEP blends were studied also at weight ratios 97.5/2.5, 90/10, and 80/20 by STEM. The overall morphology was similar to that of PS/SEP 90/10 blends. The separated micelles of SEP, which were dispersed in the PS matrix, tended to agglomerate with increasing amount of SEP. In the 80/20 blend, SEP micelles had not been separated any more, forming quite large agglomerates of irregular shape. The PP/PS/SEP 20/80/10 blends with $\lambda_{TM} = 2.5$ and 0.25 were investigated by TEM at higher magnifications. The TEM micrographs just confirmed the morphology, which had already been known from STEM.

SAXS curves were measured for all blends studied by EM and a few more, because the SAXS experiments are relatively fast and their interpretation can be straightforward if the basic morphological features are known, which was fulfilled here thanks to EM. The SAXS curve of neat PP showed a peak around $q \approx 0.04$ Å^{-1} corresponding to long period of semicrystalline polymer iPP. The SAXS curve of neat PS exhibited no peaks because aPS is an amorphous polymer. The SAXS curves of all PS/SEP blends (weight ratios 97.5/2.5, 95/5, 90/10, and 80/20) exhibited just monotonic decrease with q, indicating that aPS is amorphous and

SEP internal structure is lost. The SAXS curves of all PP/SEP blends (weight ratios 97.5/2.5, 95/5, 90/10, and 80/20) showed peaks at $q \approx 0.01$ Å^{-1} (corresponding to SEP periodic structure) and $q \approx 0.04$ Å^{-1} (associated with long period of PP), indicating that SEP internal structure is maintained even at $Z = 2.5$ wt %. The SAXS curves of all the above-described PP/PS/SEP blends were measured not only for $Z = 10$ wt %, but also for $Z = 2.5$ and 5 wt %. All the PP/PS/SEP with $Z = 2.5$ and 5 wt % displayed the same features as the corresponding curves with $Z = 10$ wt %, with two exceptions: (a) the peak at $q \approx 0.01$ Å^{-1} (connected with SEP periodicity) decreased with decreasing Z in the blends with $\lambda_{TM} = 4$ and 0.4, which is quite logical, and (b) the decrease in slope, typical of the morel structure, was not observed for $Z \leq 6.5\%$ as already discussed in the previous section.

DISCUSSION

Influence of λ_{tm} on the PP/PS blends morphology

Both theoretical considerations and numerous experimental results show that average particle size should decrease with increasing matrix viscosity. As for theory, eq. (1) predicts decrease of particle size with increasing viscosity of the matrix η_m, if all other variables remain the same (except for λ and k which depend on η_m).[7] As for experimental work, the PP/PS blends with PP matrix studied both in this work (Figs. 3(a) and 3(b)) and in the work of Fortelný et al.[25], show decrease in particle size with decreasing λ_{TM} (i.e., increasing η_m).

PP/PS blends (80/20) were prepared with $\lambda_{TM} = 4$ and $\lambda_{TM} = 0.4$. In the blends with $\lambda_{TM} = 4$, the PS particles act as hard beads, which do not break in soft PP-3 matrix. Moreover, coalescence is more intensive in the less viscous matrix of PP-3. In the blends with $\lambda_{TM} = 0.4$, the situation is just reverse: PS particles are soft, easy to break, and hard to coalesce in viscous matrix. As a result, the particles in the blend with $\lambda_{TM} = 4$ are considerably larger than those in the blend with $\lambda_{TM} = 0.4$ (cf. Figs. 3(a) and 3(b)), which accords with both theory and experiments as discussed earlier.

PP/PS blends (20/80) were prepared at two viscosity ratios: $\lambda_{TM} = 2.5$ and $\lambda_{TM} = 0.25$. The comparison of Figures 3(c) and 3(d) indicate that the theoretical assumption does not hold in this case: at least some PP particles in the blends with $\lambda_{TM} = 0.25$ are bigger than all the PP particles in the blend with higher viscosity ratio, $\lambda_{TM} = 2.5$. Despite relatively broad particle size distribution, the morphology coarseness definitely increases at lower λ_{TM}.

Various morphologies of SEP in PP/PS/SEP blends

The SEP copolymer exhibits as many as six different types of morphology in all the systems studied and as many as four different types of morphology in the PP/PS/SEP blends with compositions 80/20/10 and 20/80/10 (Table II). The various SEP morphologies are:

(i) lamellar morphology in the neat form (Fig. 1(a)),
(ii) adjacent-micellar morphology in the PP/SEP 90/10 blends,[39]
(iii) separated-micellar morphology in the PS/SEP 90/10 blends (Fig. 1(b)),
(iv) standard morphology of a compatibilizer localized mostly on the PP/PS interface in the PP/PS/SEP 20/80/10 blends with $\lambda_{TM} = 2.5$ (Fig. 5(c)),
(v) combined standard and adjacent-micellar morphology in the PP/PS/SEP 80/20/10 blends with $\lambda_{TM} = 4.0$ and 0.4 (Figs. 5(a) and 5(b)),
(vi) morel morphology in the PP/PS/SEP blends with the composition around 20/80/10 and $\lambda_{TM} = 2.5$ (Figs. 5(b), 8(b)–(d), 9(b)).

This reconfirms that the viscosity ratio, λ_{TM}, plays a very important role in the formation of PP/PS/SEP blends morphology, and consequently, in SEP compatibilizing effectiveness. λ_{TM} is given by the viscosity of the dispersed phase, η_d, and viscosity of the matrix, η_m. The viscosities are connected with the average molecular weights of the components. That is why it was possible to explain observed morphologies, using some considerations based on comparing molecular weights, M_n, and interaction parameters, χ, of the blend components, as shown in the next section.

SEP morphologies and length of polymer chains

AB block copolymer

Morphology of AB (more precisely A-block.B) block copolymer is given by T, $N\chi$, and φ (where T is temperature, N is the degree of polymerization, χ is interaction parameter, and φ is volume ratio of the block A) as described in various textbooks (e.g. Ref. 43). The neat SEP polymer, studied in this work, exhibits quite common lamellar morphology (Fig. 1(a)). It is possible to suppose that order–disorder temperature of our SEP is higher than the processing temperature of the studied blends and so the changes in SEP morphology must have occurred due to swelling forces in the blends.

Blend of homopolymer A and block copolymer AB

Let us have block copolymer AB with degree of polymerization of block A = DP(A-) = N and DP(B-) = N and homopolymer A with DP(A) = P. The morphology of AB block copolymer in the matrix of polymer A is determined by the ratio N/P[44] and by the interaction parameter, χ_{AB}, between the homopolymer and

TABLE III
Summary of Average Molecular Weights of Components of All PP/PS/SEP Blends

PP/PS/SEP blends		PS	SEP		PP
$\lambda_{TM} = 4$	Components	PS-2	S-block	EP-block	PP-3
	M_n [10^3 g/mol]	175	33	56	59
$\lambda_{TM} = 0.4$	Components	PS-1	S-block	EP-block	PP-2
	M_n [10^3 g/mol]	96	33	56	113
$\lambda_{TM} = 2.5$	Components	PS-1	S-block	EP-block	PP-2
	M_n [10^3 g/mol]	96	33	56	113
$\lambda_{TM} = 0.25$	Components	PS-2	S-block	EP-block	PP-3
	M_n [10^3 g/mol]	175	33	56	59

block B. If $N/P > 1$, then the block copolymer is solubilized by the homopolymer; in other words the swelling force is high enough to break the original morphology of the block copolymer. The final morphology of the AB copolymer depends on χ_{AB}: with increasing compatibility between homopolymer A and block B- (i.e., with decreasing χ_{AB}) the morphology may change from lamellar through micellar to homogeneous.

In all the PS/SEP blends from this work, the final morphology was always the PS matrix containing separated SEP micelles, regardless of the M_n of PS. Although the solubilization condition $N/P > 1$ was not fulfilled (see Table III), the polydispersity of the PS used was so high that at least some PS molecules had lower DP than the DP of the S-blocks and so the swelling force was high enough to break the lamellar structure of SEP. In other words, due to the high polydispersities, the $N/P > 1$ condition was fulfilled for some molecules and these molecules caused swelling of SEP, break-up of its lamellar structure and formation of the micellar structure.

All the PP/SEP blends, which were studied both in this work and in the work of Radonjič,[39] exhibited morphology of PP matrix containing adjacent SEP micelles. The solubilization of SEP occurred despite the fact that solubilization condition was not fulfilled in this case either (Table III). In analogy with the PS/SEP blends, this can be explained by relatively high polydispersities of the PP's used. However, PS/SEP blends showed separated-micellar morphology, whereas PP/SEP blends contained adjacent-micellar morphology. The difference can be attributed to certain chemical incompatibility between the PP homopolymer and EP- block of SEP, which leads to aggregation of micelles with EP- shell. In other words, the PP/SEP blend is not a system of homopolymer A and block copolymer AB, but system of homopolymer A′ and homopolymer AB, where A′ (PP homopolymer) and A (EP-block of SEP copolymer) are not identical but only compatible to some extent, which causes the aggregation of SEP micelles.

Blend of homopolymer A, homopolymer B, and block copolymer AB

Let us have block copolymer AB in a blend of polymers A and B, where DP(A-) = DP(B-) = N, DP(A) = P and DP(B) = Q. This is more general case of the situation described in the previous paragraph. Morphology of AB block copolymer in the blend is determined by the composition of the blend, by the N/P ratio, the N/Q ratio and the interaction parameter χ_{AB}. In our case, we have A = PP, B = PS, and AB = SEP, which is even more general situation because A homopolymer is not chemically identical with corresponding A-block of the copolymer and this has further consequences mentioned below.

The PP/PS/SEP 80/20/10 blend with $\lambda_{TM} = 4$ contains SEP in the form of adjacent micelles in the PP matrix. The micelles have PS-core and EP-shell. They aggregate to minimize contact between not-completely-compatible PP matrix and EP-shells of the micelles. The aggregation of micelles means that the periodic structure of SEP is preserved and corresponding peak on SAXS curve is observed. The micelles also envelope PS particles because the S-block of SEP and PS particles are compatible. Similar SEP morphology was observed in binary PP/SEP blends,[39] in which the SEP micelles aggregated as well.

The PP/PS/SEP 80/20/10 blend with $\lambda_{TM} = 0.4$ also contains adjacent micelles of SEP and the reasons why are probably the same as in the blend with $\lambda_{TM} = 4$. However, there are two important differences between the blends with $\lambda_{TM} = 4$ and 0.4: (a) the PS particles in the blend with $\lambda_{TM} = 0.4$ are approximately two times smaller and (b) the SEP is more swollen in the blend with $\lambda_{TM} = 0.4$. The first difference can be attributed to higher viscosity of the matrix in the case of PP/PS/SEP blends with $\lambda_{TM} = 0.4$; the situation is analogous to that in noncompatibilized PP/PS blends as discussed earlier. The second difference can be tentatively explained using Table III: in the blend with $\lambda_{TM} = 4$, SEP is swollen with PP-3 because its M_n is quite close to that of EP-block and not with PS-2, whose M_n is much higher than the M_n of S-block, whereas in the blend with $\lambda_{TM} = 0.4$, SEP is swollen

with both PS-1 and PP-2 as their M_n's are comparable with M_n's of S-block and EP-block, respectively. In the end the SEP copolymer is more swollen in the blend with $\lambda_{TM} = 0.4$, which is evidenced by both TEM micrographs (cf. Figs. 6(a) and 6(b)) and SAXS curves (cf. Figs. 7(a) and 7(b)).

The PP/PS/SEP 20/80/10 blend with $\lambda_{TM} = 2.5$ exhibits the standard morphology of a compatibilized binary blend: the SEP compatibilizer is localized mostly on the PP/PS interface, enveloping the PP particles. Additionally, a part of SEP seems to be dispersed in the PS matrix, both in the form of separated micelles and/or small elongated particles. These dispersed SEP particles do not tend to agglomerate because the chemical compatibility between S-shell of SEP micelles and PS matrix is perfect. Neat SEP morphology is completely broken up, because the swelling forces are high. In fact, SEP solubilization in the blend with $\lambda_{TM} = 2.5$ is the highest, because the swelling forces are as high as in the blend with $\lambda_{TM} = 0.4$ (identical homopolymers; see Table III) and, moreover, there is no incompatibility between the PS matrix and S-block.

The PP/PS/SEP 20/80/10 blend with $\lambda_{TM} = 0.25$ shows the unusual morel morphology. In Morel Structure section, it was proved that the morel morphology appears just at particular compositions and viscosity ratios. An explanation of this morphology is not easy. In any case, the dispersion of SEP compatibilizer in the blend with $\lambda_{TM} = 0.25$ is not as complete as in the case of the analogous blend with $\lambda_{TM} = 2.5$. This occurs because SEP is swollen only with PP-3 (Table III, comparable M_n's of PP-3 and EP-block) and not with PS-2 (Table III, M_n(PS) $\gg$ M_n(S-block)). As a result, the original lamellar morphology of SEP is broken, but SEP cannot be dispersed in the PS matrix, whose M_n is too high. At the same time, SEP does not tend to form particles because the S-block is chemically identical with the PS matrix. Therefore, SEP is somewhat incompletely dispersed in the PS matrix, forming thin sheets that are typical of morel morphology.

CONCLUSIONS

More than 25 PP/PS/SEP blends with a variable composition $X/Y/Z$ and variable PP/PS viscosity ratio, λ_{TM}, have been prepared. Morphology of the blends was studied using both EM and SAXS. The main objective of this work was to investigate influence of λ_{TM} on the final morphology of the blends. The following results were obtained:

- SEP is an efficient compatibilizer of PP/PS blends, as it decreases the average particle size at all studied compositions X/Y/Z and viscosity ratios λ_{TM}; the compatibilizing effectiveness of SEP is influenced by λ_{TM}.
- The viscosity ratio of the dispersed phase and matrix, λ_{TM}, changes the PP/PS/SEP morphology drastically because the morphologies of the blends differing only in λ_{TM} are very diverse.
- SEP exhibits as many as five types of different morphologies when blended with PP and/or PS. This behavior must be connected with molecular weights of polymer chains and it can be explained using thermodynamics considerations.
- It was shown that SAXS, in combination with electron microscopy techniques, can be a very efficient and time-saving method for studying polymer blends.
- A "by-product" of this work was the discovery of the brand-new type of polymer blends morphology, which was called morel structure. The characteristic feature of morel structure is the PS matrix compartmentalized by SEP.

Financial support through grants 106/02/P029 and 106/02/1248 awarded by the Grant Agency of the Czech Republic is acknowledged.

References

1. Utracki, L. A. Polymer Alloys and Blends, Thermodynamics and Rheology; Hanser Publishers: Munich, 1989.
2. Grace, H. P. Chem Eng Commun 1982, 14, 225.
3. Fortelný, I.; Živný, A. Macromol Symp 2000, 149, 157.
4. Elmendorp, J. J. In Mixing in Polymer Processing; Rauwendaal, C., Ed.; Marcel Dekker: New York, 1991.
5. Utracki, L. A. J Rheol 1991, 35, 1615.
6. Utracki, L. A.; Favis, B. D. In Handbook of Polymer Science and Technology, Vol. 4; Cheremisinoff, N. P., Ed.; Marcel Dekker: New York, 1989.
7. Wu, S. Polym Eng Sci 1987, 27, 335.
8. Serpe, G.; Jarrin, J.; Dawans, F. Polym Eng Sci 1990, 30, 553.
9. Favis, B. D.; Chalifoux, J. P. Polym Eng Sci 1987, 27, 1591.
10. Willis, L. M.; Caldas, V.; Favis, B. D. J Mater Sci 1991, 26, 4742.
11. Gonzales-Nunez, R.; Favis, B. D.; Carreau, P. J.; Lavalée, C. Polym Eng Sci 1993, 33, 851.
12. Hietaoja, P. T.; Holsti-Miettinen, R. M.; Sepälä, J. V.; Ikkala, O. T. J Appl Polym Sci 1994, 54, 1613.
13. Choi, G. D.; Jo, W. H.; Kim, H. G. J Appl Polym Sci 1996, 59, 443.
14. Mekhilef, N.; Verhoogt, H. Polymer 1996, 37, 4069.
15. Taylor, G. Proc Roy Soc A 1932, 138, 41.
16. Taylor, G. Proc Roy Soc A 1934, 146, 501.
17. Goodrich, J.; Porter, R. S. Polym Eng Sci 1967, 7, 45.
18. Lee, G. C. N.; Purdon, J. R. Polym Eng Sci 1969, 9, 360.
19. Avgeropoulos, G. N.; Weissert, F. C.; Biddison, P. H.; Böhm, G. G. A. Rubber Chem Technol 1976, 49, 93.
20. Van Puyvelde, P.; Velankar, S.; Moldenaers, P. Curr Opin Colloid Interf Sci 2001, 6, 457.
21. Fortelný, I. J Macromol Sci Phys B 2000, 39, 67.
22. Taha, M.; Frerejean, V. J Appl Polym Sci 1996, 61, 969.
23. Han, C. D.; Kim, Y. W.; Chen, S. J. J Appl Polym Sci 1975, 19, 2831.
24. Miroshnikov, Y. P.; Williams, H. L. Polym Sci USSR 1982, 24, 1811.
25. Fortelný, I.; Michálková, D.; Mikešová, J. J Appl Polym Sci 1996, 59, 155.
26. Navrátilová, E.; Fortelný, I. Polym Netw Blends 1996, 6, 127.
27. Fujiyama, H. J Appl Polym Sci 1997, 63, 1015.

28. Horák, Z.; Forť, V.; Hlavatá, D.; Lednický, F.; Večerka, F. Polymer 1996, 37, 65.
29. Hlavatá, D.; Horák, Z.; For[caron]t, V. Polym Netw Blends 1996, 6, 15.
30. Hlavatá, D.; Horák, Z.; Hromádková, J.; Lednický, F. Polym Netw Blends 1997, 7, 195.
31. Hlavatá, D.; Horák, Z.; Hromádková, J.; Lednický, F.; Pleska, A. J Polym Sci Polym Phys 1999, 37, 1647.
32. Hlavatá, D.; Horák, Z.; Hromádková, J.; Lednický, F.; Pleska, A.; Zanevsky, Yu. J Polym Sci Part B: Polym Phys 2001, 39, 931.
33. Horák, Z.; Hlavatá, D.; Fortelný, I.; Lednický, F. Polym Eng Sci 2002, 42, 2042.
34. Hlavatá, D.; Hromádková, J.; Fortelný, I.; Hašová, V.; Pleska, A. J Appl Polym Sci 2004, 92, 2431.
35. Radonjič, G.; Musil, V. Angew Makromol Chem 1997, 251, 141.
36. Radonjič, G. J Appl Polym Sci 1999, 72, 291.
37. Radonjic, G. Ph.D. Thesis; University of Maribor, Maribor, 1998; p. 141.
38. Chernenko, S. P.; Cheremukhina, G. A.; Fateev, O. V.; Smykov, L. P.; Vasiliev, S. E.; Zanevsky, Yu. V.; Kheiker, D. M.; Popov, A. N. Nucl Instrum Methods Phys Res A 1994, 348, 261.
39. Radonjič, G.; Šmit, I. J Polym Sci Part B: Polym Phys 2001, 39, 566.
40. Radonjič, G. Ph.D. Thesis; University of Maribor, Maribor, 1998.
41. Bethge, H.; Heydenreich, J. Eds; Electron Microscopy in Solid State Physics; Elsevier: Amsterdam, 1978; p. 397, Fig. 16.7.
42. Radonjic, G.; Musil, V.; Smit, I. J Appl Pol Sci 1998, 69, 2625.
43. Bower, D. I. An Introduction to Polymer Physics; Cambridge University Press, 2002; p. 365, Fig. 12.10.
44. Adedeji, A.; Hudson, S. D.; Jamieson, A. M.; Polymer 1997, 38, 737; and references cited therein.